nature chemical biology

ARTICLE

PUBLISHED ONLINE: 21 OCTOBER 2012 | DOI: 10.1038/NCHEMBIO.1094

Divergent allosteric control of the IRE1α endoribonuclease using kinase inhibitors

Likun Wang[1–4,10], B Gayani K Perera[6,10], Sanjay B Hari[6], Barun Bhhatarai[8], Bradley J Backes[1,2], Markus A Seeliger[7], Stephan C Schürer[8,9], Scott A Oakes[5], Feroz R Papa[1–4,10]* & Dustin J Maly[6,10]*

Under endoplasmic reticulum stress, unfolded protein accumulation leads to activation of the endoplasmic reticulum transmembrane kinase/endoRNase (RNase) IRE1α. IRE1α oligomerizes, autophosphorylates and initiates splicing of XBP1 mRNA, thus triggering the unfolded protein response (UPR). Here we show that IRE1α's kinase-controlled RNase can be regulated in two distinct modes with kinase inhibitors: one class of ligands occupies IRE1α's kinase ATP-binding site to activate RNase-mediated XBP1 mRNA splicing even without upstream endoplasmic reticulum stress, whereas a second class can inhibit the RNase through the same ATP-binding site, even under endoplasmic reticulum stress. Thus, alternative kinase conformations stabilized by distinct classes of ATP-competitive inhibitors can cause allosteric switching of IRE1α's RNase—either on or off. As dysregulation of the UPR has been implicated in a variety of cell degenerative and neoplastic disorders, small-molecule control over IRE1α should advance efforts to understand the UPR's role in pathophysiology and to develop drugs for endoplasmic reticulum stress–related diseases.

The UPR is an evolutionarily conserved intracellular signaling pathway triggered when unfolded proteins accumulate in the endoplasmic reticulum[1,2]. The UPR is believed to be centrally involved in the pathogenesis of numerous cell degenerative disorders such as diabetes mellitus[3] and neurodegeneration and, conversely, the inappropriate survival of secretory cell tumors such as multiple myeloma[4]. Because the UPR normally relegates irremediably endoplasmic reticulum–stressed cells to apoptosis, the ability to control the UPR's cell fate outcomes in both positive and negative directions may provide new therapeutic options for these diseases[5]. To this end, we have been developing pharmacological tools to both activate and inhibit the master regulator of the UPR, a bifunctional enzyme called IRE1α[6–8].

IRE1α is an endoplasmic reticulum transmembrane protein that becomes activated when unfolded proteins accumulate within the organelle. Through an N-terminal endoplasmic reticulum lumenal domain that senses unfolded proteins, IRE1α monomers dimerize and potentially oligomerize in the plane of the endoplasmic reticulum membrane[9–11]. This event juxtaposes cytosolic kinase domains across individual IRE1α monomers, causing *trans*-autophosphorylation. In turn, autophosphorylation activates the C-terminal RNase domain to catalyze site-specific cleavage of the mRNA encoding the XBP1 transcription factor, excising a 26-nucleotide intervening region[12,13]. Religation of cleaved XBP1 mRNA and translation in the shifted open reading frame produces the XBP1^s (where s stands for 'spliced') transcription factor, whose gene targets allow the endoplasmic reticulum to adapt to protein-folding stress.

Genetic analysis shows that activation of IRE1α's RNase is normally dependent on kinase autophosphorylation[6], but we previously identified an unusual relationship between these two domains that allows specific ligands of the kinase domain to bypass the autophosphorylation requirement and trigger RNase activation through ligand occupancy alone[14]. For instance, the orthogonal ATP-competitive inhibitor 1NM-PP1 rescues RNase activity of IRE1α mutants that lack kinase activity[7,8,14,15]. Other ligands that interact with the ATP-binding site of wild-type IRE1α also activate the RNase directly. For example, the ATP-competitive inhibitor APY29 and the clinically approved drug sunitinib activate the RNase of yeast IRE1 (ref. 16) and mouse IRE1α[7].

Given the ability to allosterically activate IRE1α's RNase through its kinase domain, we hypothesized that it may be feasible to also inhibit the RNase through the same kinase domain, but with a different class of kinase inhibitors. Two classes of kinase inhibitors, called types I and II, have been identified, which stabilize alternate kinase active site conformations in numerous protein kinase targets[17]. Here we show that a known type I kinase inhibitor and a new type II kinase inhibitor both shut down IRE1α *trans*-autophosphorylation but have divergent effects on its RNase to activate or inactivate catalytic activity, respectively. Our findings demonstrate that IRE1α RNase activity can be either up- or down-regulated through selective targeting of its kinase domain to control UPR signaling and predict that it may be possible to pharmacologically modulate other kinase-coupled enzymes in a similar way.

RESULTS

Divergent modulation of IRE1α's RNase activity

A co-crystal structure of yeast IRE1 bound with APY29, a predicted type I kinase inhibitor, shows that the kinase catalytic domain is in an active conformation, which is a conformation typically adopted by protein kinases when bound to ATP and other type I inhibitors (**Fig. 1a**)[16,18]. Moreover, two additional co-crystal structures of yeast IRE1 and human IRE1α bound with ADP show that the kinase

[1]Department of Medicine, University of California–San Francisco, San Francisco, California, USA. [2]Lung Biology Center, University of California–San Francisco, San Francisco, California, USA. [3]Diabetes Center, University of California–San Francisco, San Francisco, California, USA. [4]California Institute for Quantitative Biosciences, University of California–San Francisco, San Francisco, California, USA. [5]Department of Pathology, University of California–San Francisco, San Francisco, California, USA. [6]Department of Chemistry, University of Washington, Seattle, Washington, USA. [7]Department of Pharmacological Sciences, Stony Brook University Medical School, Stony Brook, New York, USA. [8]Center for Computational Science, University of Miami, Florida, USA. [9]Department of Molecular and Cellular Pharmacology, Miller School of Medicine, University of Miami, Florida, USA. [10]These authors contributed equally to this work. *e-mail: frpapa@medicine.ucsf.edu or maly@chem.washington.edu

domain is similarly in an active conformation[18–20]. By stabilizing IRE1α's kinase in the active conformation, these type I inhibitors act as ligands that allosterically activate its adjacent RNase domain. Therefore, we postulated that it might be possible to stabilize IRE1α's kinase domain in an alternative conformation and in so doing disable its RNase activity. To test this notion, we used a class of small-molecule kinase inhibitors that have been characterized to selectively stabilize an inactive conformation of the ATP-binding site (type II inhibitors) for a variety of kinases; examples include the clinically approved drugs imatinib and sorafenib[17,21,22]. The inactive ATP-binding site conformation stabilized by type II inhibitors is characterized by outward movement of the catalytically important aspartic acid–phenylalanine-glycine (DFG) motif and is therefore called the DFG-out conformation (**Fig. 1a**)[17,23]. In contrast, in all three co-crystal structures of IRE1 mentioned previously, the kinase domain adopts the DFG-in conformation[16,19,20].

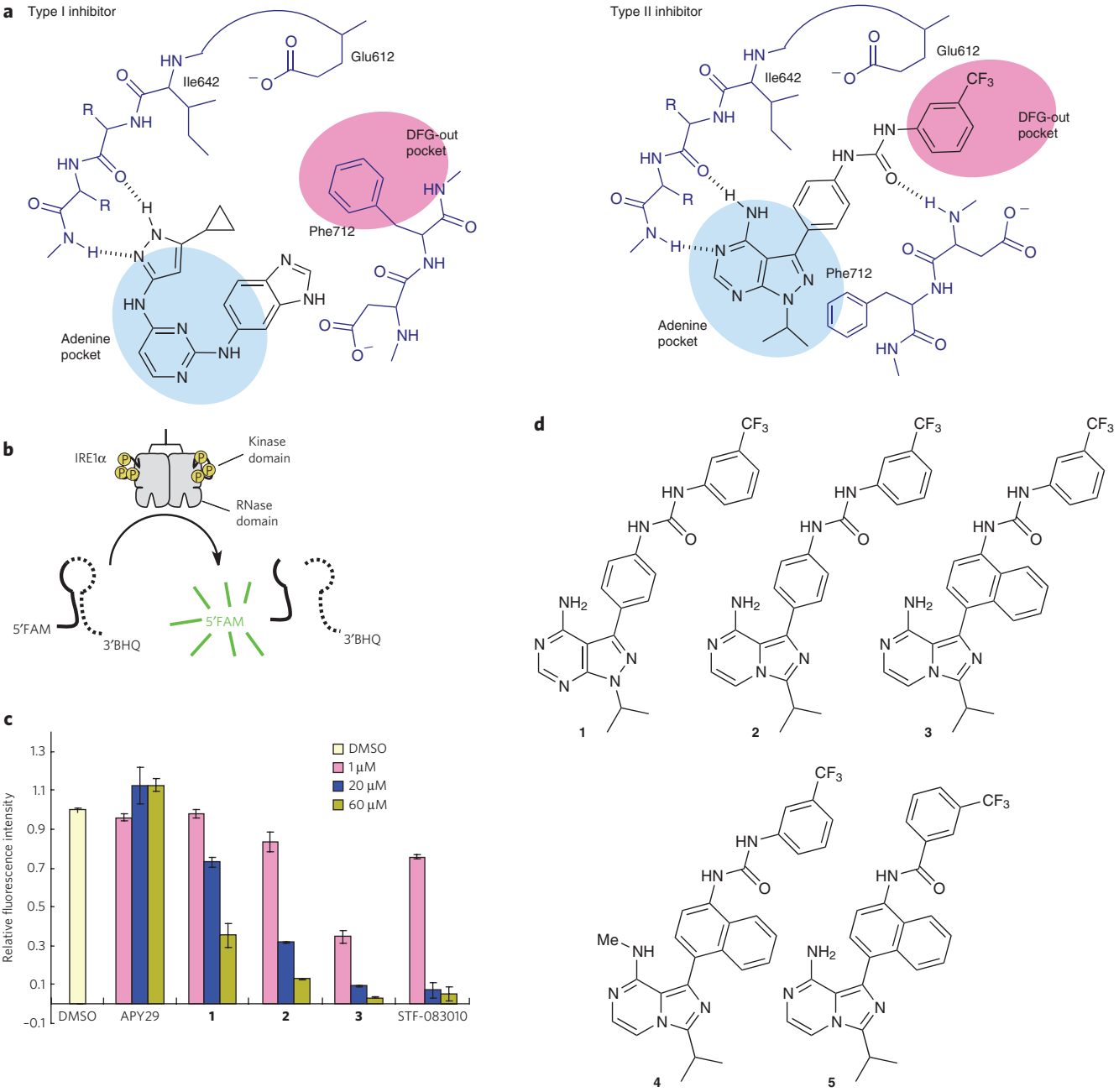

Figure 1 | Interaction of ATP-competitive inhibitors with the bifunctional kinase/RNase, IRE1α. (**a**) Proposed binding modes of type I and type II kinase inhibitors with the ATP-binding pocket of IRE1α. Left, contacts the type I inhibitor APY29 forms with yeast IRE1 (PDB code 3SDJ)[18]. Right, proposed contacts a type II inhibitor, **1**, forms with IRE1α based on the co-crystal structure of the same inhibitor bound to Src (PDB code 3EL8; **Supplementary Fig. 3**)[24]. (**b**) XBP1 RNA mini-substrate assay used for screening IRE1α modulators. IRE1α*, the recombinant human IRE1α used in the assay, spans residues 469–977, which includes the cytosolic kinase and RNase domains. Cleavage of the 5′-FAM– and 3′-BHQ–labeled XBP1 mini-substrate by IRE1α* results in FRET dequenching. (**c**) Endpoint fluorescence of IRE1α*-catalyzed cleavage reaction of XBP1 mini-substrate in the presence of varying concentrations of inhibitors or DMSO. STF-083010 is an imine-based compound that covalently inhibits the RNase domain. Relative fluorescence intensity is scaled to the signal observed with IRE1α* (1.0) or without IRE1α* (0). Data shown are mean ± s.d., $n = 3$). (**d**) Structures of the type II kinase inhibitors used in this study.

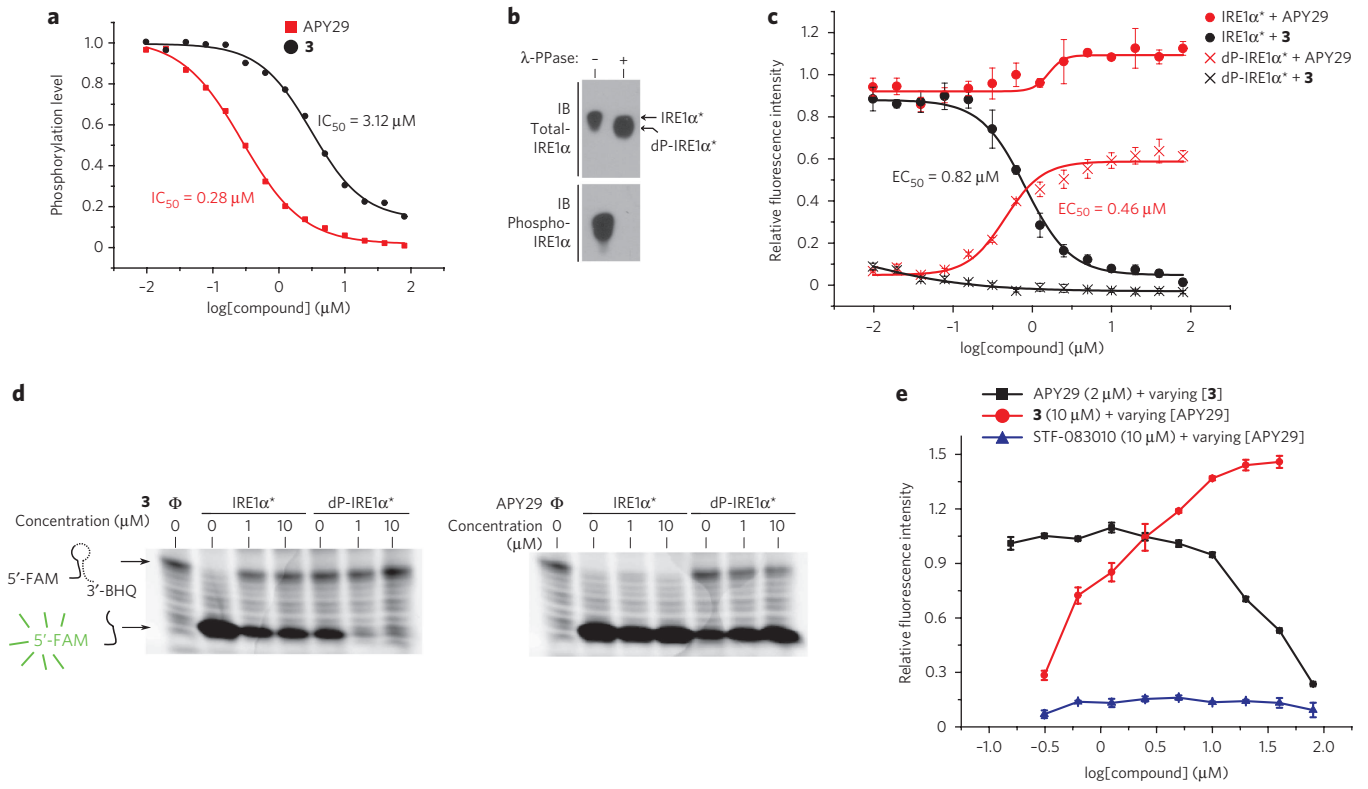

Figure 2 | APY29 and 3 divergently modulate the RNase activity and oligomerization state of IRE1α*. (**a**) Inhibition of IRE1α* autophosphorylation *in vitro* by APY29 and **3**. Normalized autophosphorylation levels and IC_{50} values for both compounds are shown. (**b**) λ-PPase treatment of IRE1α* produces dephosphorylated IRE1α* (dP-IRE1α*). Immunoblots (IBs) using IRE1α-specific and phosphoIRE1α-specific antibodies are shown. (**c**) RNase activities of IRE1α* and dP-IRE1α* under varying concentrations of APY29 or **3**. Assays were performed using the conditions described in **Figure 1b**. Half-maximum effective concentration (EC_{50}) values were determined by fitting normalized fluorescence intensities (mean ± s.d., $n = 3$). (**d**) Urea PAGE of XBP1 mini-substrate cleavage by IRE1α* and dP-IRE1α* with and without **3** or APY29. ϕ indicates no IRE1α* or dP-IRE1α*. (**e**) RNase competition assays between APY29 and **3**. The red line shows IRE1α* RNase activity under fixed **3** and varying APY29 concentrations. The black line shows IRE1α* RNase activity under fixed APY29 and varying **3** concentrations. The blue line shows IRE1α* RNase activity under fixed STF-083010 and varying APY29 concentrations (mean ± s.d., $n = 3$).

Therefore, we hypothesized that stabilizing an inactive ATP-binding site conformation of IRE1α with type II inhibitors may have inhibitory rather than activating allosteric effects on the RNase. To this end, several previously characterized type II inhibitors were screened for their ability to block the RNase activity of a recombinant soluble human IRE1α mini-protein construct containing the kinase/RNase domains called IRE1α* (**Supplementary Results**, **Supplementary Figs. 1** and **2**). As IRE1α* is basally autophosphorylated, its RNase is autoactive and can be assayed using a fluorescence resonance energy transfer (FRET)-quenched XBP1 RNA mini-substrate[7] (**Fig. 1b**). Although all of the compounds we tested with this assay contain the core binding elements predicted to stabilize the DFG-out conformation, only one ligand, **1**, showed measurable inhibition of IRE1α*'s RNase activity (**Fig. 1c**,**d**). Compound **1** is a pyrazolopyrimidine-based inhibitor that has been shown to stabilize the DFG-out conformation of the nonreceptor tyrosine kinases Src and Abl[24]. Proposed contacts with IRE1α, based on the co-crystal structure of **1** bound to Src (Protein Data Bank (PDB) code 3EL8)[24], are shown in **Figure 1a**.

Despite its modest activity, **1** served as a promising starting point to develop more potent allosteric RNase inhibitors. A number of similar analogs were generated and tested for RNase inhibition. Although most modifications of **1** were deleterious, replacing the pyrazolopyrimidine scaffold with an imidazopyrazine core provided an appreciable increase in overall potency (**2**; **Fig. 1c**,**d**). Furthermore, substituting the 4-anilino group at the C3 position of **2** with a naphthylamine moiety provided **3**, the most potent compound identified in this study. Notably, **3** inhibits XBP1 RNA cleavage to a similar degree as STF-083010, an imine-based small molecule that directly inhibits the IRE1α RNase through covalent modification[25].

Similarly to APY29, **3** shows dose-dependent reduction of IRE1α* kinase autophosphorylation *in vitro* (**Fig. 2a** and **Supplementary Fig. 4**). Thus, although **3** and APY29 are both IRE1α* kinase inhibitors, they have opposing effects on its RNase activity, with APY29 acting as a slight activator. To further characterize the differences between the two kinase inhibitors, we generated a version of IRE1α* with low basal RNase activity by using λ-phosphatase (λ-PPase) to remove activating phosphates from the enzyme (**Fig. 2b** and **Supplementary Fig. 5**). As expected, the dephosphorylated variant of IRE1α* (dP-IRE1α*) has substantially lower basal RNase activity than IRE1α*; incubating dP-IRE1α* with increasing APY29 concentrations progressively restores its ability to cleave the XBP1 mini-substrate, reaching a plateau at ~60% of the activity of IRE1α* (**Fig. 2c**,**d** and **Supplementary Fig. 6**). In contrast, **3** suppresses the residual RNase activity of dP-IRE1α*.

Competition experiments were performed to further explore the opposing effects of APY29 and **3**. Increasing concentrations of APY29 progressively reverse IRE1α* RNase inhibition caused by a fixed concentration of **3** (**Fig. 2e**). In contrast, increasing concentrations of **3** restore RNase inhibition in the setting of a fixed concentration of APY29, with an expected increase in the half-maximum inhibitory concentration (IC_{50}; **Fig. 2e** and **Supplementary Fig. 7**). As predicted, APY29 cannot rescue direct inhibition caused by the

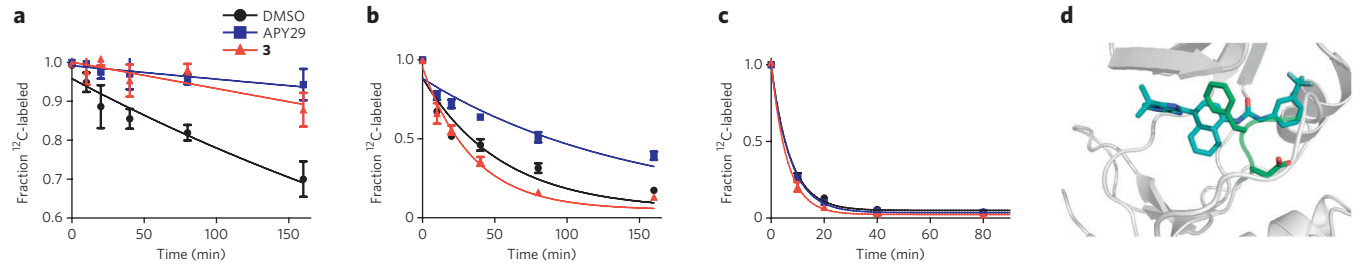

Figure 3 | Characterization of 3′s interaction with the ATP-binding site of IRE1α. (**a**–**c**) Results of the ICAT footprinting experiments with IRE1α*. Alkylation rates were measured in the presence of DMSO (black), APY29 (blue; 20 μM) or **3** (red; 20 μM) (mean ± s.d., *n* = 3). Alkylation rate of Cys645 (LCAATLQEYVEQK) (**a**). Alkylation rate of Cys715 (AMISDFGLCK) (**b**). Alkylation rate of Cys572 (ISFCPK) (**c**). (**d**) A molecular model of **3**′s interaction with the ATP-binding site of IRE1α (gray). IRE1α is in the DFG-out inactive conformation. The imidazopyrazine ring of **3** (cyan) occupies the adenine pocket, and the 3-(trifluoromethyl)phenyl urea occupies the DFG-out pocket. The DFG motif is shown in green. No favorable poses for **3** bound to the DFG-in conformation of IRE1α could be determined.

covalent RNase modifier STF-083010. Taken together, these results strongly suggest that APY29 and **3** exert their opposing effects on RNase activity through the same binding site.

The drug sunitinib is a promiscuous type I inhibitor that has been shown to inhibit the kinase activity of yeast and human IRE1α[16,19]. To investigate the differences between **3** and other ATP-competitive inhibitors of IRE1α, we further characterized the interaction of sunitinib with our IRE1α* and dP-IRE1α* constructs. As expected, sunitinib is a dose-dependent inhibitor of the autophosphorylation activity of IRE1α* (**Supplementary Fig. 8a**). In addition, sunitinib activates the RNase activity of dP-IRE1α*, which is consistent with its type I pharmacophore (**Supplementary Fig. 8b**). Therefore, both APY29 and sunitinib stabilize an ATP-binding site conformation that activates the RNase domain of IRE1α. Like APY29, sunitinib can be added in increasing amounts to rescue the RNase activity of IRE1α* in the presence of a fixed concentration of **3** (**Supplementary Fig. 8c**). Together, these results show that **3** opposes the stereotypical RNase activation shown by various type I ATP-competitive inhibitors of IRE1α.

Analysis of the 3-IRE1α and APY29-IRE1α interactions

To further confirm that AYP29 and **3** exert their opposing effects through the same ATP-binding site, we next turned to a series of biochemical footprinting experiments[26,27]. Specifically, the accessibility of three native cysteine residues within human IRE1α (Cys572, Cys645 and Cys715) to alkylating agents in the presence or absence of APY29 and **3** was determined (**Supplementary Fig. 9**). For these studies, electrophilic isotope-coded affinity tag (ICAT) reagents were used to allow a ratiometric and, therefore, quantitative comparison of alkylation rates[27]. As Cys645 and Cys715 are located within the ATP-binding cleft of IRE1α, their accessibility is expected to be affected by ligands that occupy this site, whereas Cys572 is a solvent-exposed residue located on the top of the N-terminal lobe of the kinase. Consistent with both APY29 and **3** occupying the ATP-binding site of IRE1α, Cys645, which is located in the kinase hinge region, is highly shielded from alkylating agents in the presence of either inhibitor (**Fig. 3a**). In contrast, these inhibitors exert opposing effects on the accessibility of Cys715, with APY29 slowing the rate of alkylation and **3** increasing it. Cys715 is located in the activation loop of IRE1α (two residues C-terminal to the DFG motif), and the divergent influence of APY29 and **3** on this residue is concordant with these ligands stabilizing different conformations of the activation loop (**Fig. 3b**). As expected, no detectable difference in the accessibility of Cys572, which is distal to the kinase active site of IRE1α, is observed in the presence of either inhibitor (**Fig. 3c**).

Next, we performed molecular docking experiments to obtain a better understanding of how **3** and APY29 interact with the ATP-binding site of human IRE1α. A model of the DFG-in ATP-binding site conformation was generated from a co-crystal structure of human IRE1α bound to ADP (PDB code 3P23, chain A)[19]. As a structure of IRE1α in the DFG-out conformation has not yet been described, a homology model of this conformation was generated by using the activation loop of another kinase, the tyrosine kinase Abl2, as a template. Both the DFG-in and DFG-out models were optimized using multistep all-atom minimization and explicit water molecular dynamics simulations[28]. Predictably, the docked structure of APY29 bound to the DFG-in conformation of human IRE1α is similar to that of APY29 bound to the yeast IRE1 enzyme (**Supplementary Fig. 10**)[16]. The pyrazole ring of APY29 forms hydrogen bonds with the kinase hinge region, and the pyrimidine moiety occupies the adenine pocket. Attempts to obtain a favorable pose of APY29 bound to the DFG-out conformation

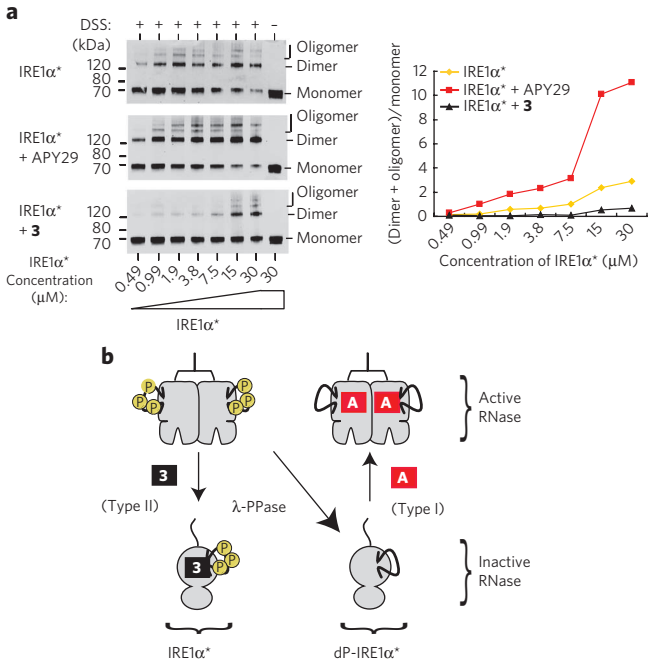

Figure 4 | APY29 and 3 differentially affect the oligomerization state of IRE1α*. (**a**) Left, immunoblots of IRE1α* after treatment with the crosslinker disuccinimidyl suberate (DSS; 250 μM). Increasing concentrations of IRE1α* were incubated with DMSO, APY29 (200 μM) or **3** (200 μM). Right, quantification of the ratios of oligomeric to monomeric IRE1α*. (**b**) Model of how type I and type II kinase inhibitors affect the RNase activities and oligomeric states of IRE1α* and dP-IRE1α*. A, APY29; **3**, type II inhibitor **3**.

of IRE1α were unsuccessful, which is consistent with the ability of this ligand to exclusively stabilize the active conformation of the ATP-binding site.

The most favorable docking pose for 3 bound to the DFG-out conformation of IRE1α is shown in **Figure 3d**. In this pose, the imidazopyrazine ring of this ligand forms two hydrogen bonds with the hinge region and occupies the adenine pocket. The bulky naphthyl ring of 3 adopts an almost-orthogonal conformation relative to the core scaffold and stacks against the isoleucine gatekeeper residue. Like other type II inhibitors, the trifluoromethylphenyl moiety of 3 occupies the hydrophobic pocket created by movement of the phenylalanine side chain in the DFG motif. Although 3 is well accommodated in the DFG-out conformation of human IRE1α, no favorable poses were observed for this inhibitor bound to the DFG-in conformation. Indeed, our docking studies predict that the only way that 3 can bind IRE1α without movement of the DFG motif in the activation loop is if the inhibitor disrupts canonical interactions with the hinge region of the kinase.

To further experimentally test our docking model, we generated analogs of 3 that contain structural elements predicted to lower inhibitor potency (4 and 5; **Fig. 1d**). Compound 4 contains an N-methyl group that is predicted to disrupt its interaction with the hinge region of IRE1α, and the amide linkage of 5 should not allow the trifluoromethylphenyl moiety to form as favorable interactions with the hydrophobic pocket created by movement of the DFG motif. Consistent with our model, both 4 and 5 show a markedly diminished ability to inhibit the RNase activity of IRE1α compared to 3 (**Supplementary Fig. 11**).

APY29 and 3 divergently affect IRE1α oligomerization

Self-association of kinase/RNase monomers has been reported to increase RNase activity as dimers, higher-order oligomers or both form in yeast and mammalian IRE1 proteins[10,16,19]. Although it has not been resolved whether IRE1α RNase activation requires kinase dimerization or high-order oligomerization *per se*, it is generally accepted that monomeric species are inactive; furthermore, the degree of order may correlate directly with activity[16]. Thus, we used APY29 and 3 to test the prediction that they would divergently affect the oligomerization state of human IRE1α as a basis for their opposing effects on its RNase activity. Specifically, we predicted that RNase activators should drive monomers into higher-order species (dimers and perhaps oligomers). To test this prediction, we incubated increasing concentrations of IRE1α* with either DMSO or saturating concentrations of APY29 or 3, and we determined the ratio of oligomeric (defined as all species greater than monomers (dimers and oligomers)) to monomeric IRE1α (**Fig. 4a**). In the absence of ligands, IRE1α* shows a concentration-dependent increase in the oligomer/monomer ratio. The presence of APY29 further enhances—whereas 3 decreases—this concentration-dependent increase in the IRE1α* oligomer/monomer ratio. Taken together, our *in vitro* data support a model in which these two classes of kinase inhibitors divergently modulate IRE1α* RNase activity by exerting opposing effects on the oligomerization state of the enzyme (**Fig. 4b**).

IRE1α mutants show increased sensitivity to 3

Having used a truncated form of IRE1α for all of our *in vitro* studies, we next turned to cell-based experiments to test whether we could replicate divergent modulation of the full-length IRE1α transmembrane protein with the two classes of kinase inhibitors. We first tested and confirmed the on-target effects of 3 using IRE1α chemical-genetic systems we had previously developed[7]. Specifically, we used tetracycline-inducible isogenic T-REx 293 stable cell lines expressing either wild-type or a 'holed' IRE1α gatekeeper mutant^{I642A} that contains an enlarged ATP-binding pocket to determine whether 3 is able to block the RNase activity of IRE1α *in vivo*. Induced with

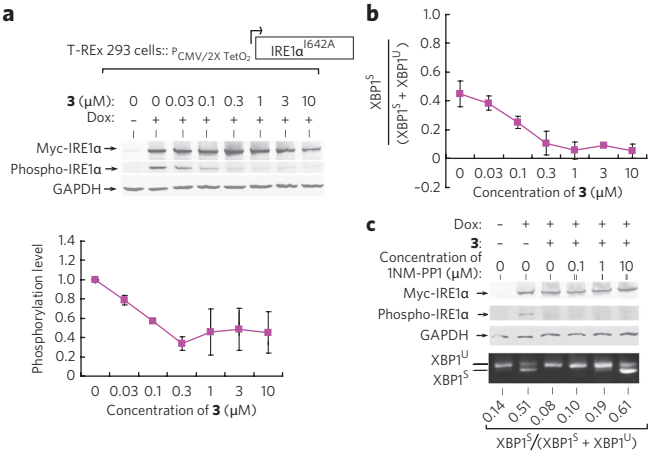

Figure 5 | Chemical-genetic modulation of IRE1α kinase and RNase activity *in vivo*. (**a**) Immunoblots for total IRE1α (Myc-IRE1α) and phospho-IRE1α in T-REx 293 cells expressing IRE1α^{I642A} under Dox control. GAPDH, glyceraldehyde 3-phosphate dehydrogenase. Cells were pretreated for 1 h with 3 at indicated concentrations, then induced with Dox (1 μM) for 8 h. Plots show normalized phosphorylation levels and ratios of spliced XBP1 mRNA under varying concentrations of 3 (mean ± s.d., n >3). (**b**) Quantification of the XBP1 cDNA amplicons from the cells described in **a**. Ethidium bromide–stained agarose gels are shown in **Supplementary Figure 16**. XBP1^S, spliced XBP1; XBP1^U, unspliced XBP1. (**c**) Competition between the bumped kinase inhibitor 1NM-PP1 and 3 against IRE1α^{I642A}. T-REx 293 cells expressing IRE1α^{I642A} were pretreated for 1 h with 3 (1 μM) plus or minus varying concentrations of 1NM-PP1 before Dox induction (1 μM) for 8 h. Quantification shows ratios of spliced XBP1 mRNA as a function of 3 and 1NM-PP1 concentrations.

doxycycline (Dox), the transgenic wild-type IRE1α or IRE1α^{I642A} spontaneously clusters in the endoplasmic reticulum and *trans*-autophosphorylates and splices XBP1 mRNA, without requiring upstream endoplasmic reticulum stress (**Fig. 5a** and **Supplementary Figs. 12** and **13**). As expected, 3 inhibits autophosphorylation and XBP1 mRNA splicing in the wild-type cell lines (**Supplementary Fig. 13a**,**b**). Consistent with these inhibitory effects occurring through a direct interaction with IRE1α, control compound 4 does not affect either of these parameters, even at the highest concentration tested (**Supplementary Fig. 13c**). Furthermore, we hypothesized that the enlarged ATP-binding pocket of IRE1α^{I642A} would better accommodate the bulky C3 substituent of 3, leading to enhanced sensitivity. Indeed, our docking studies suggest that the naphthyl ring of 3 is able to occupy a hydrophobic pocket that is accessible in IRE1α^{I642A} and not the wild-type protein (**Supplementary Fig. 14**). Confirming this notion, low nanomolar concentrations of 3 are sufficient to completely block autophosphorylation and XBP1 splicing through this mutant (**Fig. 5a**,**b** and **Supplementary Figs. 15** and **16**). Furthermore, increasing concentrations of the type I 'bumped' inhibitor 1NM-PP1, which is selective for mutant kinases that contain alanine or glycine gatekeeper residues, is able to rescue the RNase activity of IRE1α^{I642A} in the presence of 3 (**Fig. 5c** and **Supplementary Fig. 17**).

Our data suggest a model for IRE1α^{I642A}, which can be activated merely through overexpression to basally splice ~50% of cellular XBP1 mRNA, that 1NM-PP1 further increases, whereas 3 reduces, the activity of the RNase (**Supplementary Fig. 18**). We propose that these divergent effects proceed from the stabilization of the kinase active site in two distinct modes by these inhibitors, with 1NM-PP1 acting on the holed IRE1α^{I642A} kinase in a similar fashion as APY29 acts on wild-type IRE1α. In summary, the type II pharmacophore 3 most likely enforces an inactive kinase conformation in IRE1α^{I642A} as

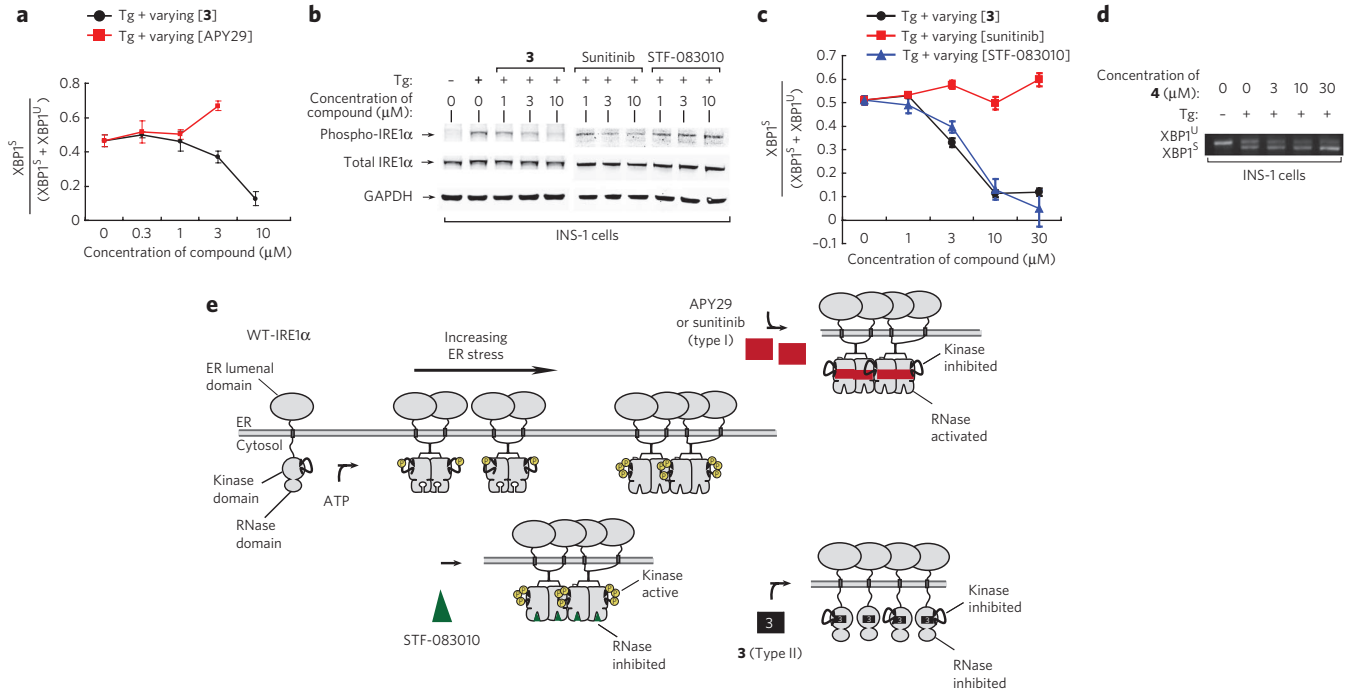

Figure 6 | Divergent modulation of endogenous IRE1α RNase activity under endoplasmic reticulum stress with type I and type II kinase inhibitors. (**a**) Quantification of ethidium bromide–stained agarose gel of XBP1 cDNA amplicons from INS-1 cells pretreated for 1 h with **3** or APY29 at indicated concentrations, followed by thapsigargin (Tg, 6 nM) for 4 h. Ratios of $XBP1^S$ over ($XBP1^S$ + $XBP1^U$) are plotted (mean ± s.d., n = 3). Gels are shown in **Supplementary Figure 19**. (**b**) Immunoblots for total IRE1α and phospho-IRE1α using extracts from INS-1 cells pretreated for 1 h with **3**, sunitinib or STF-083010 at indicated concentrations, followed by treatment with thapsigargin (6 nM) for 2 h. GAPDH, glyceraldehyde 3-phosphate dehydrogenase. (**c**) Quantification of ethidium bromide–stained agarose gel of XBP1 cDNA amplicons from the INS-1 cells described in **b**. Gels are shown in **Supplementary Figure 20**. (**d**) Ethidium bromide–stained agarose gel of XBP1 cDNA amplicons from INS-1 cells pretreated for 1 h with **4** at indicated concentrations, followed by treatment with thapsigargin (6 nM) for 4 h. (**e**) Model of how type I kinase inhibitors (APY29 or sunitinib), type II kinase inhibitors (**3**) and RNase inhibitors (STF-083010) modulate the enzymatic activities of wild-type IRE1α. APY29 inhibits IRE1α *trans*-autophosphorylation but promotes oligomerization and activates the RNase domain. STF-083010 inhibits the RNase activity of IRE1α but does not affect kinase activity or the overall oligomerization state. Compound **3** inhibits both the kinase and RNase domains of IRE1α and stabilizes the monomeric form. It should be noted that these cartoons are not meant to differentiate between the relative orientations of monomer subunits in IRE1α.

it does with wild-type IRE1α. Furthermore, **3** may stabilize monomeric $IRE1\alpha^{I642A}$, whereas 1NM-PP1 may promote oligomerization, as APY29 does for the wild-type IRE1α (**Fig. 4b**).

3 blocks both enzymatic activities of IRE1α *in vivo*

To further explore how IRE1α modulators affect the kinase and RNase activities of endogenous IRE1α under endoplasmic reticulum stress, we next turned to *in vivo* studies using INS-1 rat insulinoma cell lines, which are derived from insulin-producing pancreatic β-cell tumors and contain large well-developed endoplasmic reticula. These cells were treated with the endoplasmic reticulum SERCA ATPase pump inhibitor thapsigargin at concentrations to induce endoplasmic reticulum stress and IRE1α activation that cause ~50% of cellular XBP1 mRNA to be spliced (**Fig. 6a** and **Supplementary Fig. 19**). Recapitulating our *in vitro* results, **3** and APY29 have opposing dose-dependent effects on endoplasmic reticulum stress–induced activation of the RNase of endogenous IRE1α (**Fig. 6a** and **Supplementary Fig. 19**). Furthermore, **3** abrogates IRE1α autophosphorylation at a similar concentration as that needed for it to block RNase activity (**Fig. 6b**,**c** and **Supplementary Figs. 20** and **21**). Control compound **4** does not block the splicing of XBP1 mRNA (**Fig. 6d** and **Supplementary Fig. 22**). Consistent with its *in vitro* activity, the type I inhibitor sunitinib is able to partially inhibit the kinase activity of IRE1α, but it has no effect on the RNase activity of this enzyme (**Fig. 6b**,**c** and **Supplementary Figs. 20** and **21**) at the concentrations tested. The RNase inhibitor STF-083010 was also tested in INS-1 cells that had been treated with thapsigargin. As expected, STF-083010 inhibits XBP1 splicing in a dose-dependent manner but does not prevent IRE1α autophosphorylation (**Fig. 6b**,**c** and **Supplementary Figs. 20** and **21**). Therefore, **3** is the only compound identified to date that has the ability to block both enzymatic activities of IRE1α, *in vitro* and *in vivo* (**Fig. 6e**).

DISCUSSION

Recent studies show that the duration and amplitude of UPR activation powerfully affect both cell function and fate[7,8,29,30]. Indeed, many cell-degenerative diseases such as diabetes mellitus feature increased endoplasmic reticulum stress and UPR activation in affected cells[3,31,32]. These same markers are evident in a wide range of solid and hematopoietic malignancies[33]. Properly ascertaining the role of the UPR in these disease contexts will require development of tool compounds that target critical nodes in the UPR in both positive and negative directions. The master UPR regulator IRE1α, which controls cell fate under endoplasmic reticulum stress, offers two enzymatic targets that could be modulated with small molecules. In this work, we exploited the unusual mechanistic relationship between these two catalytic domains to inhibit the RNase from a distance by inhibiting the kinase.

Starting with known pharmacophores that stabilize an inactive conformation in other protein kinases, we optimized a type II inhibitor lead to produce **3**. Despite inhibiting IRE1α kinase autophosphorylation similarly to the type I inhibitor APY29, **3** inhibits XBP1 mRNA splicing, even during endoplasmic reticulum stress. Consistent with competition studies, footprinting experiments

strongly suggest that 3 and APY29 bind the same ATP-binding pocket. However, these same footprinting experiments indicate that these inhibitors cause divergent effects on the activation loop of IRE1α and support a model in which 3 and APY29 promote distinct, mutually exclusive movements of the DFG motif contained within the activation loop.

The aforementioned experiments, combined with modeling studies, lead to a parsimonious model of IRE1α modulation by kinase inhibitors (**Fig. 6e**) that posits that the protein can adopt either a canonical DFG-in or a DFG-out conformation, as is seen with other kinases under the influence of types I and II inhibitors, respectively. However, whereas for other kinases these two distinct modes of inhibition stereotypically shut down kinase function, for the multidomain kinase IRE1α, the two inhibition modes have opposite and divergent results on the attached RNase activity. To our knowledge, this ability to modulate a second catalytic activity in a multidomain kinase in two different directions with distinct classes of ATP-competitive inhibitors has not been reported to date. We expect that this ability may be extended to many of the other known multidomain kinases.

Notably, opposite effects on oligomeric state were found using the two compounds: type I inhibitors increase the dimeric and possibly oligomeric state of IRE1α and the catalytic activity of the RNase, whereas type II inhibitors decrease both in tandem. Given previous reports of a direct mechanistic relationship between the degree of order and RNase activity in IRE1 proteins[16], we speculate that the inactive conformation that 3 stabilizes in IRE1α promotes the monomeric state.

It is of course conceivable that a different, previously unidentified active site conformation is adopted in the presence of 3; fully resolving this particular point in the future will require atomic-level co-crystal structures. Regardless, the particular kinase active site conformation stabilized by 3 has the unique and previously unreported property of preserving the mechanistic coupling between the kinase and the RNase in IRE1α, allowing full inhibition of both activities in concert. We propose that this represents a new alternative to aldehyde-based covalent inhibitors of the RNase such as STF-083010 (or another recently reported compound called 4μ8C[34]), which leave kinase autophosphorylation and oligomerization intact. In contrast to the action of direct RNase inhibitors, any biological signaling through the kinase that is dependent on phosphorylation of nonautonomous substrates or kinase-mediated scaffolding should be simultaneously quenched with type II kinase inhibitors.

In summary, the ability to now inhibit the effector RNase domain of IRE1α with type II kinase inhibitors complements our previous ability to activate the RNase with type I inhibitors, independent of upstream endoplasmic reticulum stress, establishing opposite directions of control over this master UPR regulator. Thus, type II kinase inhibitors of IRE1α will expand on a tool kit that includes chemical-genetic systems to test and validate the UPR's role in endoplasmic reticulum stress–related diseases. Although 3 is not completely selective for IRE1α over other protein kinases, this compound serves as a starting point for the generation of more potent and selective inhibitors that may eventually be developed into disease-modifying drugs for endoplasmic reticulum stress–related disorders. Moreover, the ability to toggle the IRE1α RNase on and off through its kinase domain may serve as a precedent for pharmacologically targeting the many other kinase-coupled enzymes present in eukaryotes.

METHODS

Synthesis and characterization of probes are described in the **Supplementary Methods**.

Expression and purification of IRE1α* and dP-IRE1α*. A construct containing the cytosolic kinase and RNase domains of human IRE1α (residues 469–977, IRE1α*) was expressed in SF9 insect cells by using the Bac-to-Bac baculovirus expression system (Invitrogen) with a His_6 tag at the N terminus and purified with a nickel–nitriloacetic acid (Qiagen) column. To generate dP-IRE1α*, we removed basal phosphorylation sites by incubating IRE1α* with λ-PPase (New England Biolabs) at a molar ratio of 5:1 (IRE1α*/λ-PPase) in 50 mM HEPES pH 7.5, 100 mM NaCl, 1 mM $MnCl_2$, 2 mM dithiothreitol (DTT) and 0.01% Brij 35 detergent (v/v) for 40 min at 23 °C. Dephosphorylation was verified by immunoblotting with an antibody specific for phosphoIRE1α.

Kinase assays. Inhibitors (initial concentration 80 μM, two-fold serial dilutions) were incubated with IRE1α* in cleavage buffer (20 mM HEPES at pH 7.5, 0.05% Triton X-100 (v/v), 50 mM potassium acetate, 1 mM magnesium acetate, 1 mM DTT) for 20 min, followed by incubation with 10 μCi [γ-^{32}P]ATP (3,000 Ci mmol^{-1}, PerkinElmer) at 23 °C for 30 min. Samples were then separated by SDS-PAGE and autoradiographed. The autophosphorylation level was quantified by setting the band intensity of IRE1α* without compound treatment as 1 and the background as 0.

***In vitro* RNase assay.** 5′-Carboxyfluorescein (FAM)- and 3′-Black Hole Quencher (BHQ)-labeled XBP1 single stem-loop mini-substrate (5′FAM-CUGAGUCCG CAGCACUCAG-3′BHQ) were purchased from Dharmacon. We incubated 0.2 μM IRE1α* or dP-IRE1α* with inhibitors or DMSO for 20 min in cleavage buffer, followed by incubation with 3 μM RNA substrate for 5 min. The reaction was quenched by adding urea to a final concentration of 4 M, and the fluorescence was detected on a SpectraMax M5 microplate reader (Molecular Devices) with excitation and emission wavelengths of 494 nm and 525 nm, respectively. The fluorescence intensities were normalized by setting the signal for the reaction with IRE1α* and DMSO to 1 and the reaction without IRE1α* to 0. The cleavage products were also resolved by urea PAGE after phenol-chloroform extraction and ethanol precipitation. Internally ^{32}P-labeled mouse XBP1 RNA was also used as a substrate, as described[7].

ICAT footprinting. Heavy and light iodonated ICAT reagents were made as described in ref. 27. Purified human Ire1α was exchanged into 50 mM Tris (pH 8.0), 50 mM KCl, 5 mM $MgCl_2$ and 0.5 mM tris(2-carboxyethyl)phosphine. One 3 μM stock solution was divided into three solutions, and each was mixed with either DMSO, APY29 or 5 to yield solutions containing 1% (v/v) DMSO and 20 μM of inhibitor. Heavy labeling reagent was added to the protein solutions, and 25-μl aliquots were taken at specified times and quenched with excess DTT. Samples were precipitated with 0.2% sodium deoxycholate and 10% trichloroacetic acid (w/v) on ice for 10 min. The mixtures were centrifuged at 4 °C for 15 min, and pellets were washed with cold acetone. The pellets were then resuspended in 30 μl of 200 mM Tris (pH 8.0), 7 M urea and 2.4 mM light labeling reagent, and they were incubated in the dark for 30 min. The solutions were diluted with 210 μl 200 mM Tris (pH 8.0), 5.7 mM $CaCl_2$, 0.5 μg porcine trypsin (1-tosylamido-2-phenylethyl chloromethyl ketone–treated; Sigma) and 125 ng Glu-C endoproteinase (Roche), and they were incubated at 23 °C overnight. Samples (0.3 pmol) were injected onto a Thermo Scientific Dionex Acclaim Pepmap100 NanoLC capillary column (C_{18}, 150-mm length, inner diameter 75 μm, 3-μm particle size) connected inline to a Finnigan LCQ mass spectrometer. Peptides of interest were identified by MS/MS data (Sequest), and corresponding XIC peaks were integrated. Alkylation curves were fit using GraphPad Prism software.

IRE1α* crosslinking to determine oligomer to monomer ratio. Increasing concentrations of IRE1α* (0.49–30 μM) were incubated with DMSO, 3 (200 μM) or APY29 (200 μM) for 20 min and then crosslinked by adding 250 μM disuccinimidyl suberate (Pierce) for 1 h at 23 °C in cleavage buffer. The reaction was quenched by addition of 50 mM Tris-HCl (pH 7.5). The samples were then boiled, resolved on SDS-PAGE and immunoblotted for IRE1α with an antibody specific for IRE1α (visualization and quantification with a LI-COR Odyssey scanner).

Cell culture and XBP1 mRNA splicing. INS-1 cells were grown in RPMI, 10% FBS buffer (v/v), 1 mM sodium pyruvate, 10 mM HEPES, penicillin-streptomycin, 2 mM glutamine and 50 μM β-mercaptoethanol. T-REx 293 IRE1α or IRE1α^{I642A} were grown in DME H-21 with 10% FBS buffer (v/v) and penicillin-streptomycin. After 1 h incubation with compounds, INS-1 cells were treated with 6 nM thapsigargin for 4 h, and T-REx 293 IRE1α-expressing cells were treated with 1 μM Dox for 8 h. The RNA was then extracted using RNeasy Mini Kit (Qiagen) and reverse transcribed using the QuantiTect Reverse Transcription Kit (Qiagen). XBP1 splicing was performed as previously described[7]. Primers used: sense primer rXBP 1.3S (5′- AAACAGAGTAGCAGCACAGACTGC-3′) and antisense primer rXBP 1.2AS (5′- GGATCTCTAAGACTAGAGGCTTG GTG-3′) for the INS-1 cell line and sense primer mXBP1.3S (5′-AAACAGAGT AGCAGCGCAGACTGC-3′) and antisense primer mXBP1.2AS (5′-GGATCTC TAAAACTAGAGGCTTGGTG-3′) for the T-REx 293 cell line. PCR products were resolved on 2.5% (w/v) agarose gels, stained with ethidium bromide and quantified by ImageJ.

Statistical analysis. All experiments were performed in triplicate, unless otherwise specified. Results are shown as mean ± s.d.

Other methods. Detailed information is available in the **Supplementary Methods**.

Received 13 July 2012; accepted 10 September 2012; published online 21 October 2012

References

1. Walter, P. & Ron, D. The unfolded protein response: from stress pathway to homeostatic regulation. *Science* **334**, 1081–1086 (2011).
2. Merksamer, P.I. & Papa, F.R. The UPR and cell fate at a glance. *J. Cell Sci.* **123**, 1003–1006 (2010).
3. Scheuner, D. & Kaufman, R.J. The unfolded protein response: a pathway that links insulin demand with β-cell failure and diabetes. *Endocr. Rev.* **29**, 317–333 (2008).
4. Carrasco, D.R. *et al.* The differentiation and stress response factor XBP-1 drives multiple myeloma pathogenesis. *Cancer Cell* **11**, 349–360 (2007).
5. Tabas, I. & Ron, D. Integrating the mechanisms of apoptosis induced by endoplasmic reticulum stress. *Nat. Cell Biol.* **13**, 184–190 (2011).
6. Tirasophon, W., Welihinda, A.A. & Kaufman, R.J. A stress response pathway from the endoplasmic reticulum to the nucleus requires a novel bifunctional protein kinase/endoribonuclease (Ire1p) in mammalian cells. *Genes Dev.* **12**, 1812–1824 (1998).
7. Han, D. *et al.* IRE1α kinase activation modes control alternate endoribonuclease outputs to determine divergent cell fates. *Cell* **138**, 562–575 (2009).
8. Han, D. *et al.* A kinase inhibitor activates the IRE1α RNase to confer cytoprotection against ER stress. *Biochem. Biophys. Res. Commun.* **365**, 777–783 (2008).
9. Credle, J.J., Finer-Moore, J.S., Papa, F.R., Stroud, R.M. & Walter, P. On the mechanism of sensing unfolded protein in the endoplasmic reticulum. *Proc. Natl. Acad. Sci. USA* **102**, 18773–18784 (2005).
10. Zhou, J. *et al.* The crystal structure of human IRE1 luminal domain reveals a conserved dimerization interface required for activation of the unfolded protein response. *Proc. Natl. Acad. Sci. USA* **103**, 14343–14348 (2006).
11. Gardner, B.M. & Walter, P. Unfolded proteins are Ire1-activating ligands that directly induce the unfolded protein response. *Science* **333**, 1891–1894 (2011).
12. Calfon, M. *et al.* IRE1 couples endoplasmic reticulum load to secretory capacity by processing the XBP-1 mRNA. *Nature* **415**, 92–96 (2002).
13. Yoshida, H., Matsui, T., Yamamoto, A., Okada, T. & Mori, K. XBP1 mRNA is induced by ATF6 and spliced by IRE1 in response to ER stress to produce a highly active transcription factor. *Cell* **107**, 881–891 (2001).
14. Papa, F.R., Zhang, C., Shokat, K. & Walter, P. Bypassing a kinase activity with an ATP-competitive drug. *Science* **302**, 1533–1537 (2003).
15. Lin, J.H. *et al.* IRE1 signaling affects cell fate during the unfolded protein response. *Science* **318**, 944–949 (2007).
16. Korennykh, A.V. *et al.* The unfolded protein response signals through high-order assembly of Ire1. *Nature* **457**, 687–693 (2009).
17. Liu, Y. & Gray, N.S. Rational design of inhibitors that bind to inactive kinase conformations. *Nat. Chem. Biol.* **2**, 358–364 (2006).
18. Korennykh, A.V. *et al.* Cofactor-mediated conformational control in the bifunctional kinase/RNase Ire1. *BMC Biol.* **9**, 48 (2011).
19. Ali, M.M. *et al.* Structure of the Ire1 autophosphorylation complex and implications for the unfolded protein response. *EMBO J.* **30**, 894–905 (2011).
20. Lee, K.P. *et al.* Structure of the dual enzyme Ire1 reveals the basis for catalysis and regulation in nonconventional RNA splicing. *Cell* **132**, 89–100 (2008).
21. Wan, P.T. *et al.* Mechanism of activation of the RAF-ERK signaling pathway by oncogenic mutations of B-RAF. *Cell* **116**, 855–867 (2004).
22. Schindler, T. *et al.* Structural mechanism for STI-571 inhibition of abelson tyrosine kinase. *Science* **289**, 1938–1942 (2000).
23. Ranjitkar, P., Brock, A.M. & Maly, D.J. Affinity reagents that target a specific inactive form of protein kinases. *Chem. Biol.* **17**, 195–206 (2010).
24. Dar, A.C., Lopez, M.S. & Shokat, K.M. Small molecule recognition of c-Src via the Imatinib-binding conformation. *Chem. Biol.* **15**, 1015–1022 (2008).
25. Papandreou, I. *et al.* Identification of an Ire1α endonuclease specific inhibitor with cytotoxic activity against human multiple myeloma. *Blood* **117**, 1311–1314 (2011).
26. Tu, B.P. & Wang, J.C. Protein footprinting at cysteines: probing ATP-modulated contacts in cysteine-substitution mutants of yeast DNA topoisomerase II. *Proc. Natl. Acad. Sci. USA* **96**, 4862–4867 (1999).
27. Underbakke, E.S., Zhu, Y. & Kiessling, L.L. Isotope-coded affinity tags with tunable reactivities for protein footprinting. *Angew. Chem. Int. Ed. Engl.* **47**, 9677–9680 (2008).
28. Bowers, K.J. *et al.* in *Proceedings of the ACM/IEEE Conference on Supercomputing (SC06)* (Tampa, Florida, USA, 2006).
29. Yoshida, H. *et al.* A time-dependent phase shift in the mammalian unfolded protein response. *Dev. Cell* **4**, 265–271 (2003).
30. Lu, P.D. *et al.* Cytoprotection by pre-emptive conditional phosphorylation of translation initiation factor 2. *EMBO J.* **23**, 169–179 (2004).
31. Huang, C.J. *et al.* High expression rates of human islet amyloid polypeptide induce endoplasmic reticulum stress–mediated β-cell apoptosis, a characteristic of humans with type 2 but not type 1 diabetes. *Diabetes* **56**, 2016–2027 (2007).
32. Oyadomari, S. *et al.* Targeted disruption of the Chop gene delays endoplasmic reticulum stress-mediated diabetes. *J. Clin. Invest.* **109**, 525–532 (2002).
33. Feldman, D.E., Chauhan, V. & Koong, A.C. The unfolded protein response: a novel component of the hypoxic stress response in tumors. *Mol. Cancer Res.* **3**, 597–605 (2005).
34. Cross, B.C. *et al.* The molecular basis for selective inhibition of unconventional mRNA splicing by an IRE1-binding small molecule. *Proc. Natl. Acad. Sci. USA* **109**, E869–E878 (2012).

Acknowledgments

This work was supported by the US National Institutes of Health Director's New Innovator Award DP2 OD001925 (F.R.P.), RO1 DK080955 (F.R.P.), RO1 CA136577 (S.A.O.), R00 GM080097 (M.A.S.) and R01 GM086858 (D.J.M.), an American Cancer Society Research Scholar Award (S.A.O.) and the Burroughs Wellcome (F.R.P.), Juvenile Diabetes Research (F.R.P.) and Sloan (D.J.M.) Foundations. S.B.H. was supported by a predoctoral fellowship from the American Heart Association.

Author contributions

F.R.P. and D.J.M. contributed equally as senior authors to the study. F.R.P. and D.J.M. conceived the idea and designed the study. With the guidance of F.R.P. and D.J.M., L.W. designed and performed the biochemical and cellular studies. B.G.K.P. designed and performed all of the chemical syntheses. S.B.H. performed footprinting experiments. B.B. and S.C.S. performed molecular modeling studies. All authors designed experiments, analyzed data and commented on the manuscript. F.R.P. and D.J.M. cowrote the paper.

Competing financial interests

The authors declare no competing financial interests.

Additional information

Supplementary information and chemical compound information is available in the online version of the paper. Reprints and permissions information is available online at http://www.nature.com/reprints/index.html. Correspondence and requests for materials should be addressed to F.R.P. or D.J.M.